EU contract number RII3-CT-2003-506395 CARE-Report-2008-014-HIPPI

HIPPI-Relevant Activities at IAP-Frankfurt on the Development of the Room Temperature CH-DTL Second Report

G. Clemente[1], H. Podlech[1], U. Ratzinger[1] R. Tiede[1], S. Minaev[2]

1) Institute for Applied Physics, J.W. Goethe University, Frankfurt am Main, Germany
2) ITEP, Moscow, Russia

1 Introduction

The tasks of IAP in the frame of the CARE-HIPPI activities are concentrated on the development of room temperature Crossbar H-Type (CH) - DTL's. These activities go in parallel with the R&D performed on the FAIR Proton Injector, which will be the first linac operated with such a cavity.

The first steps were concentrated on the simulations of the general RF properties of the cavity such as shunt impedance, Q-value, resonance frequency and field distributions. Even if the results were extremely encouraging, showing significant higher shunt impedance in the low and medium β range with respect to classical DTLs, the crossbar geometry presented many points to be investigated in terms of construction, cooling and copper plating.

For this reason it was planned to build a first cold model aiming to work out the required technical solutions for the practical realisation of the cavity. As a second step the construction of a first prototype able to stand high RF power was scheduled. In parallel the beam dynamics design of the FAIR Proton Injector was investigated carefully, in order to reach the required parameters for the foreseen antiproton programs at GSI.

This initial plan was changed during the term of HIPPI: motivated by the promising simulations results and pushed by the overall progress of the FAIR Project, the first model went much further than scheduled. The cavity was successfully copper plated at GSI and it was fully equipped with an efficient cooling system. It was tested with 2kW cw end of 2006. The test was very successful and the cavity would have stand full power up to the sparking limit, if a pulsed rf power amplifier at 339 MHz would have been available. So it could formally be called “CH Prototype 1” instead of “Cold Model”, in order to be in accordance to the HIPPI WP2 milestones and deliverables lists. The results achieved on “CH Prototype 1” were summarized in CARE-Note-2007-001-HIPPI, released at the beginning of 2007.

During HIPPI the idea of coupled CH cavities was born, as a way to exploit the 2.5 MW rf power provided by commercial amplifiers. As a consequence, our “CH Prototype 2” is now the 1:2 scaled model of the FAIR Proton Linac Cavity 2. It is a cavity consisting of two CH sections coupled by a DTL-type lens.

The mechanical design and rf tuning work performed on this cavity are one of the main topics of the present report and are likewise one of our major steps in CH-DTL cavity design and construction within the framework of HIPPI. “CH Prototype 2” is the basis for the full prototype of FAIR Proton Linac Cavity 2. The full scale prototype fabrication will be ordered in summer 2008. This shows that the CH cavity development has progressed quite well during EU-FP6 within the framework of HIPPI.

2 The FAIR Proton Injector

The FAIR antiproton physics program requires an intensity up to 7 10^{10} pbar/h which, taking into account the pbar production and cooling rate, implies a primary proton beam of 2 10^{16} p/h. This intensity is much beyond the capabilities of the existing UNILAC and, for this reason a dedicated proton linac has to be developed to deliver the required primary proton beam to the SIS18/100 synchrotron complex (Fig.1).

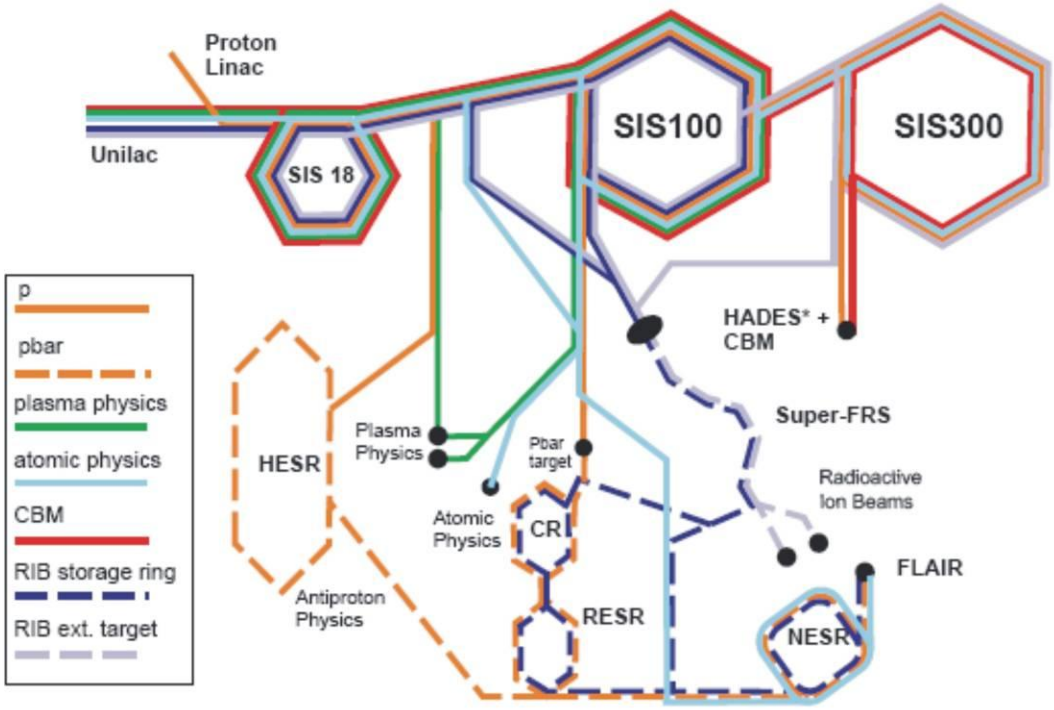

Fig.1: Illustration of the parallel beam operation at FAIR showing the iter for the production of antiprotons.

The primary proton beam intensity is limited by the Space Charge Limit of the SIS18, which can be expressed as,

$$N_{SIS} = 4.305\ 10^{13}\ \beta^2\gamma^3$$

while the pbar rate is dominated by the stochastic cooling time which is proportional to the particle number if a sufficiently high signal/noise ratio is assumed.

An output energy of 70 MeV allows to get close to the saturation of pbar production while a further increase in energy doesn't bring any significant advantage apart from a small decrease of the SIS100 cycle time since the cooling time becomes now longer; moreover, fixing the final energy at 70 MeV avoids any jumps in RF frequency which results in a considerably cost saving.

The choice of frequency for a linac in this energy range results from the compromise between the requirements of minimized radial defocusing at low energy, which is proportional to the frequency itself, and the RF efficiency which, for room temperature structures, scales as the square root of the frequency. For those reasons all linacs in such an energy range are operated at frequencies between 300 and 400 MHz which results to be an adequate compromise.

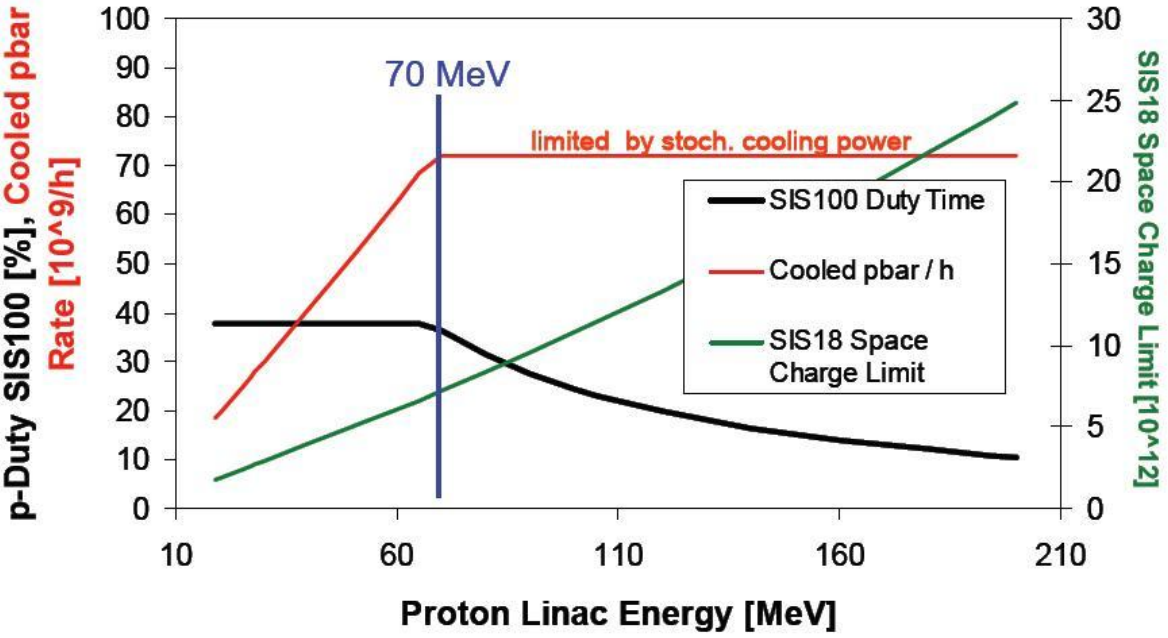

Fig.2: Dependences of the space charge limit of proton beams in the SIS18 (green curve) and corresponding relative duty time for primary proton beam delivery by the SIS100 (black) as function of the proton linac energy. The achievable rate of cooled pbars is presented by the blue curve.

Additionally, the LEDA project in Los Alamos has successfully demonstrated the proton acceleration at beam currents up to 100 mA with a 350 MHz RFQ. The original choice for the GSI proton linac foresaw the use of the 352.2 MHz, 1.1 MW, CERN klystrons recovered from the dismounted LEP. Finally, after the development of commercial 324 MHz, 2.5 MW Toshiba klystrons for JPARC, the linac frequency was set to 325.2 MHz which is also exactly three times the frequency of the existing 108.4 MHz GSI UNILAC. In this way the entire GSI injector system will be based on multiple of the same basic frequency of 36 MHz (the operating frequency of the UNILAC High Current Injector HSI).

Finally, taking into account the space charge limit of the SIS18 and considering that the proton beam will fill around 60 % of the horizontal emittance of this synchrotron via Multiturn Injection, is it possible to demonstrate that the normalised brilliance requirements corresponds to

$$B_n = 12.4 \text{ mA}/\mu\text{m}$$

i.e. 2.1 μm at the injection current of 35 mA and 4.2 μm at the design current of 70 mA

The scheme of the 325 MHz, 70 MeV FAIR proton injector is sketched in Fig.3: an ECR source delivers up to 100 mA proton beam which is accelerated by an RFQ up to energy of 3 MeV. In a first step 35 mA will be accelerate within a 70 μs RF pulse into the main linac composed of 12 CH-type cavities grouped in 6 pairs of coupled structure. At the intermediate energy of 35 MeV around 1 meter will be left to host a complete diagnostic section.

The CH-DTL, under development at the Frankfurt University, which represents the extension of well established Interdigital H-cavities (IH) to frequency higher than 250 MHz. Like the IH this structure is characterised by the lack of internal focusing elements which allows the construction of extremely compact cavities characterized by higher shunt impedance when compared to conventional RF structure (Fig.4). In Tab.1 the main parameters of the FAIR Proton injector are listed.

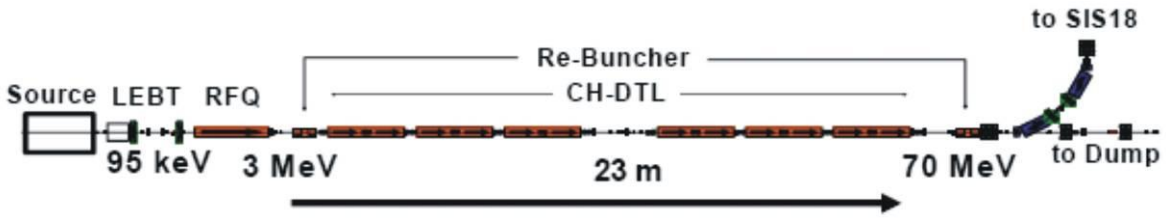

Fig.3: The layout of the FAIR Proton Injector.

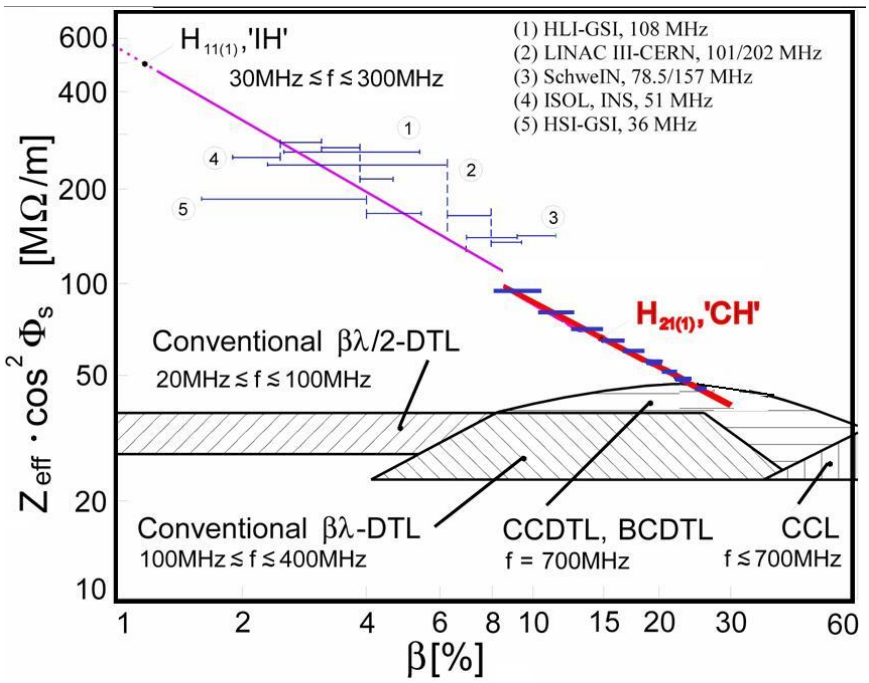

Fig.4: The effective shunt impedance of existing structures and the expected one of the FAIR Proton Injector

Length [m]	30
Output Energy[MeV]	70
Peack Current [mA]	35 (70 design)
Protons per Pulse [10^{12}]	7.8
Beam Pulse Length [μs]	36
Repetition Rate [Hz]	4
Frequency [MHz]	325.244
Longitudinal rms emitt. [keV ns]	17
Norm. Transverse rms emitt. [μm]	4.2
Duty Factor [%]	0.2

Tab.1: The main parameters of the FAIR proton injector.

2 The Coupled CH: the CCH-DTL

2.1 Basic Concept

As already explained the main linac will be fed by 6 klystons operated below the saturation value of 3.0 MW: this large availability of power pushes in the direction of coupled structures in order to match the linac with such a high availability of power. The starting point to develop a coupling between two resonators of the CH type is the role of the electromagnetic lens which has to be placed between the resonators to ensure the beam focusing. A possible solution is to place the lens outside the tank and to add a coupling port to transfer the RF wave from one resonator to the other: this would lead to a scheme similar to the Cell Coupled Linac. The other possibility is to develop a concept based on a coupling section which includes the triplet: in this way the construction results easier and more efficient.

A possible application of this concept is shown in Fig.5 which illustrates the RF current flow that would create the desired coupling. The RF current on the lens outer cylinder is oriented parallel along the beam axis while the closest stems of the CH resonators present opposite charge status resulting in a coupling cell of lens N $\beta\lambda$.

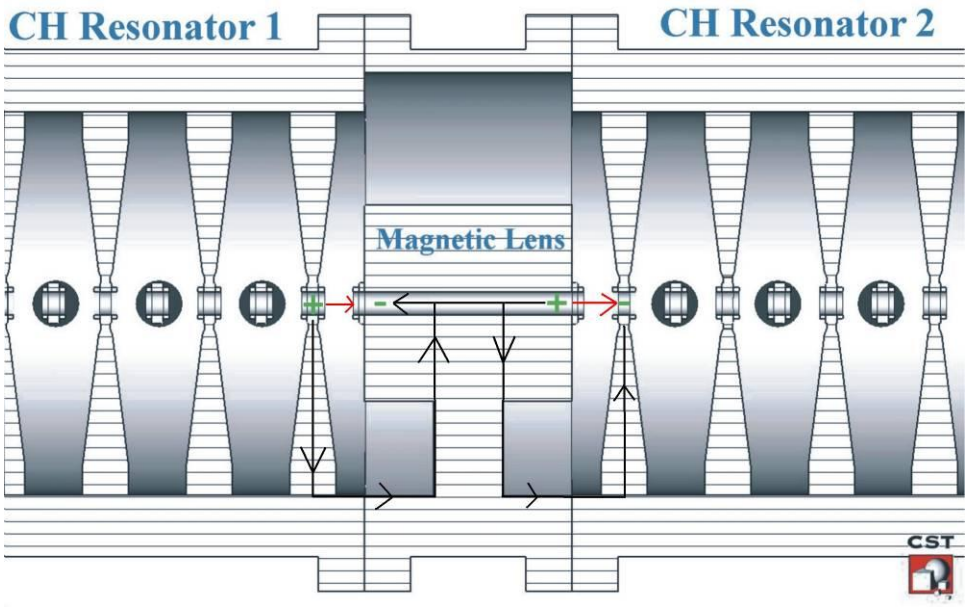

Fig.5: The coupled scheme between two CH resonators: the illustrated current flow creates a 0-Mode coupling.

To understand how to concretize this concept, one can start from the geometry of a single CH resonator shown in Fig.6; the analysis of the magnetic flux in the end cells shows how the magnetic field surrounds the last half drift tubes emulating the field distribution of a cavity exited in E_{010} mode.

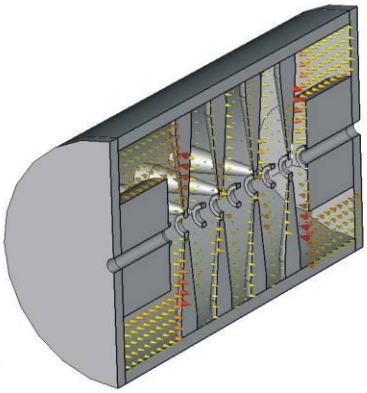

Fig.6: The magnetic flux on the cavity middle plane of a single CH-DTL

If one suppose to put together two CH-DTL of that type and to replace the end walls by a radial support for the lens, the result in terms of magnetic flux will be the one described in Fig.7, where the magnetic field runs parallel and anti parallel to beam axis in the CH modules to then surround the focusing elements (as it is in the classical DTL's exited by the E010 Mode). This corresponds exactly to an RF current on the outer cylinder of the lens which is oriented parallel to the beam axis.

Finally, since the three resonators, the 2 CH-DTL's and the coupling cell, must resonate at the same frequency, the radius of each component has to be adjusted independently so that each resonator has the same resonance frequency. The result is a compact structure where two H_{211} resonators are electromagnetically coupled by an intertank section which oscillates in the E_{010} Mode: the magnetic field generated by the incoupling loop placed in the middle of the intertank section penetrates in both resonators exiting them in the TEM mode.

This solution presents many advantages with respect any solution based on slots and aperture which could have been adopted by the Cell Coupled Linac: the construction is very simple, requiring only the insertion of the magnetic lens inside the coupling element and the modules can be easily opened to perform any kind of maintenance. Moreover, there is a large experience with this kind of tube installation inside IH cavities.

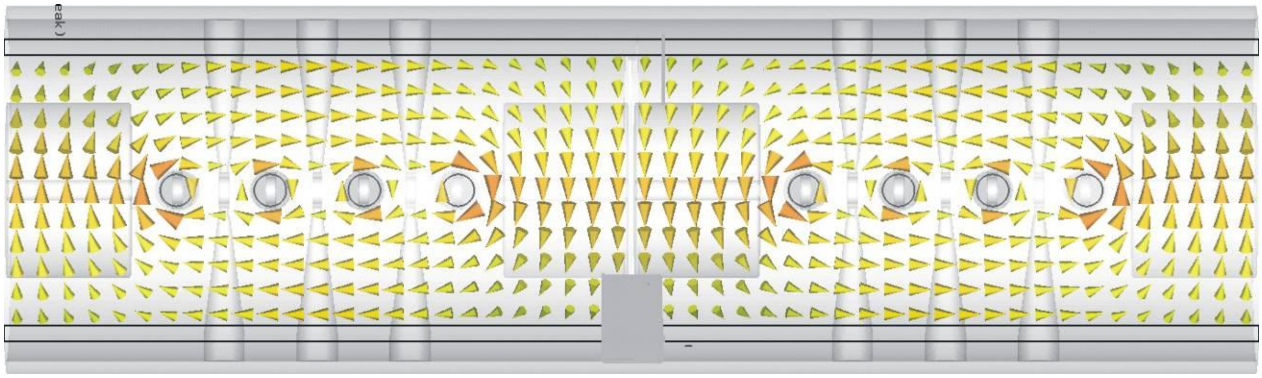

Fig. 7: The magnetic field distribution at half radius of a system made by 2 CH resonators where the inner walls are replaced by a simple radial support for the lens place between the cavities

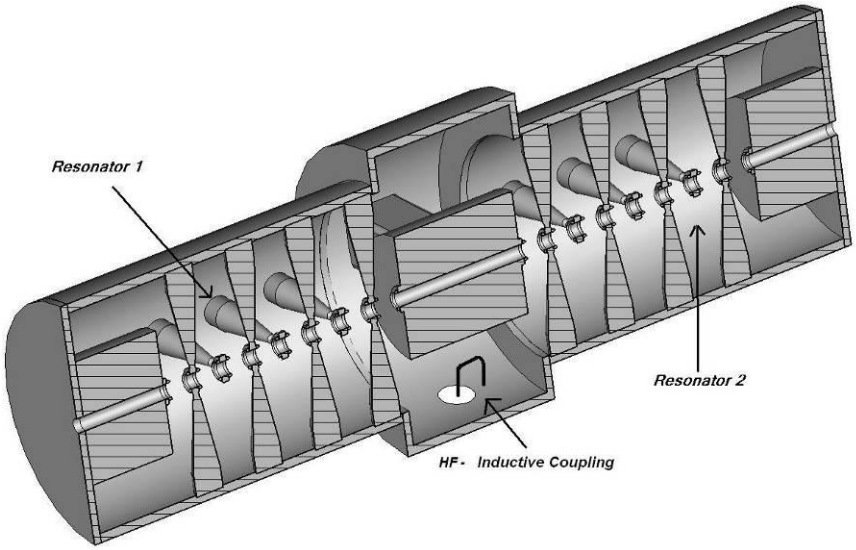

Fig.8: The coupled CH-DTL.

3 The Second Resonator of the Proton Injector

3.1 General Parameters

To definitely proof this innovative coupling concept, it was decided to investigate the second resonator of the GSI Proton Injector, i.e. the coupled third and fourth tanks: the choice to analyze the second module, and not for example the first one, is dictated by the fact that the final design of the RFQ is, at the moment, still not fixed. In this way still some degrees of freedom are left in order to potentially change the first module, only it's initial and final energy being fixed. In a first step, the LORASR code was employed to design the main parameters such as the number of gaps, voltage distribution, tube length and transit time factors. Finally, Microwave Studio was employed to optimize the geometry and to tune the field distribution inside the cavity.

This three meters long cavity consists of 29 gaps in total, 13 in the first CH resonator and 14 in the second one: as explained in the previous section the coupling is ensured by an intertank section housing the magnetic triplet needed for the beam focusing.

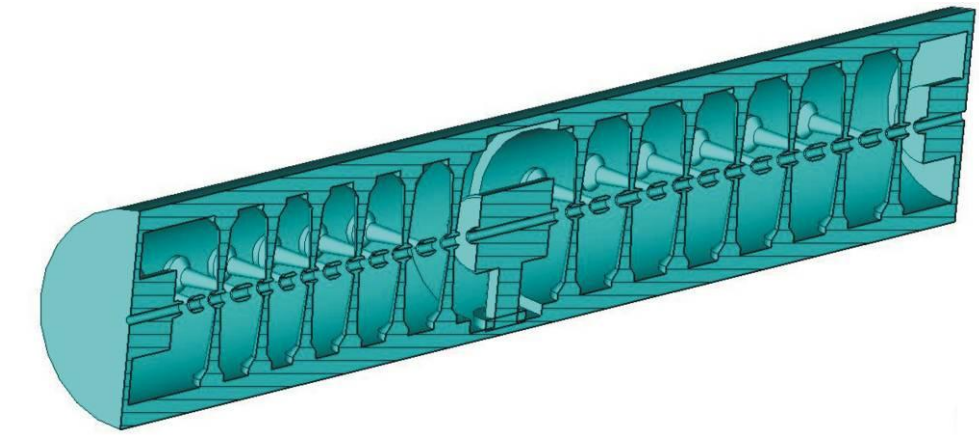

Fig.9: The second resonator of the GSI proton injector.

The first resonator has a length of 1.18 meters for an inner diameter of 184.5 mm: it holds a total voltage of 7.2 MV with an average effective gradient of 6.4 MV/m. The second resonator is longer, 1.45 meter with a larger inner diameter of 189 mm: the applied voltage of 7.2 MV corresponds to an average effective gradient of 5.8 MV/m. The coupling cell has a diameter of 214 mm and hosts the 24 cm long lens; the distance between the centre of the last gap of the first CH and the centre of the first gap of the second one is 2 $\beta\lambda$ calculated at the transit energy of 17.4 MeV.

The end cells are characterised by a quite large end half drift tube which is used to tune the cavity and to host a first quadrupole and a phase probes.

The applied effective voltage is shown in Fig.13 together with the transit time factors as calculated by LORASR: these parameters were employed to calculate the length of the drift tubes in order to obtain a homogeneous electric field on the axis which is expected to be around 12 MV/m.

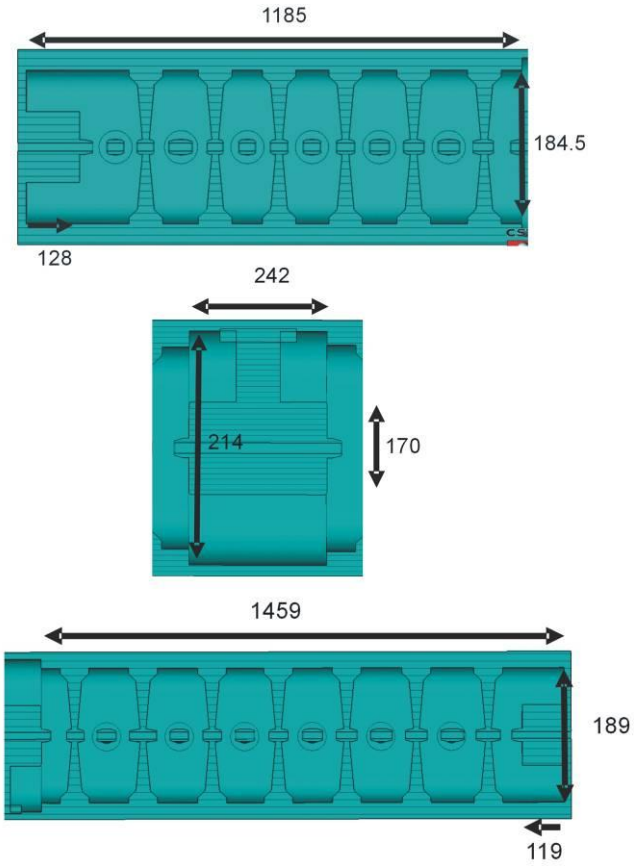

Fig.10: The main dimension of the second resonator of the FAIR Proton Injector

No. of gaps	27 (13+14)
Frequency [MHz]	325.2
Energy range [MeV]	11.7-24.3
beam loading [kW]	882.6
Heat Loss [MW]	1.35
Total Power [MW]	2.2
Q_0-Value	15300
Effective Shunt Impedance [MΩ/m]	60
Average E_0T [MV/m]	6.4 - 5.8
Kilpatrick Factor	2.0
Coupling Constant [%]	0.3
No. of Plungers	11 (4+1+6)
Beam Aperture [mm]	20
Total Length [mm]	3000

Tab.2: The main parameters of the second resonator of the GSI proton injector.

3.2 Details of construction

3.2.1 The stems

The stems are designed on the basis of a conical shape ending with a cylinder in the connection region with the outer tank. There are several reasons which justify this solution:

- A conical shape allows larger stem radius in the contact point with the outer cylinder, where the welding takes place: this ensure a higher mechanical stability.
- The contact line between the stems and the outer cylinder bears a high current density and should be large enough to avoid overheating during RF operation.
- The reduction of the radius along the stems corresponds to a reduction in the mutual capacitance between each couple of stems avoiding a reduction in the efficiency of the machine.
- With respect to any solutions involving profile steps, the copper plating becomes much easier for this design.

In order to keep the construction as simple as possible the stem shape remains unchanged in both resonators as well as the ratio between the inner and the outer diameter of the drift tubes which is fixed at 1.3 all along the structure.

The choice to use an inner diameter of 20 mm results from the compromise to optimize the RF efficiency, which decreases for larger aperture, and the necessity to avoid beam loss which pushes towards larger aperture.

Error studies performed with LORASR have demonstrated the validity of such a choice. Finally, a 36 mm corona surrounds the tubes in order to provide mechanical stability during the welding operations and to leave enough space for the water channel. It is important to remark that the contact region between the stems and the drift tubes will be subject to a strong mechanical stress during the welding procedure of the stem inside the outer cylinder: for this reason this region must be enough robust to avoid a potential deformation of the drift tubes.

3.2.2 The Cooling System

If on one side the geometry of the CH is really suitable for an optimum cooling of the stems, on the other hand the high current flow on the surface of the enclosing walls makes necessary to the outer cylinder as well: since one cannot use and internal girder, a new solution has to be found. There are two feasible possibilities:

- 4 water pockets are mounted on the outer wall;
- a double walled outer cylinder is used.

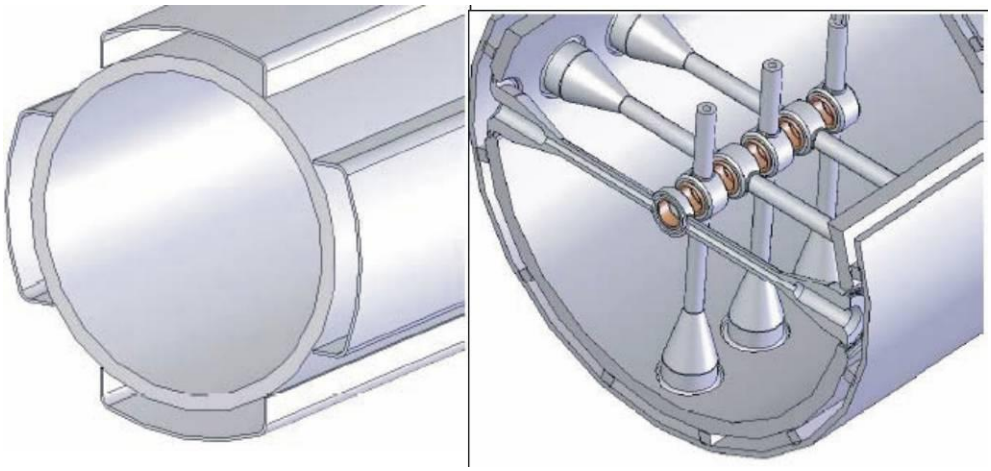

Fig.11: Two proposed solutions for the cooling system of the CH-DTL as proposed by the NTG Company.

This last solution has the main advantage that the stems and the outer cylinder can be cooled by the same channel but, on the other side, it is much more complicated and expensive.

The proposal to use external water pipes is very easy, cheap and doesn't require any further welding since the channel can be screwed on the top of the cavity. In this case each stem has its own water connection ensuring an optimal cooling system all along the machine; this solution was used on the test model built at IAP and tested under high power (2 kW, cw).

During this test no significant change in frequency was observed demonstrating that the cavity didn't suffer from thermal deformation induced by the Ohmic heating. This proofs the validity of the proposed cooling system.

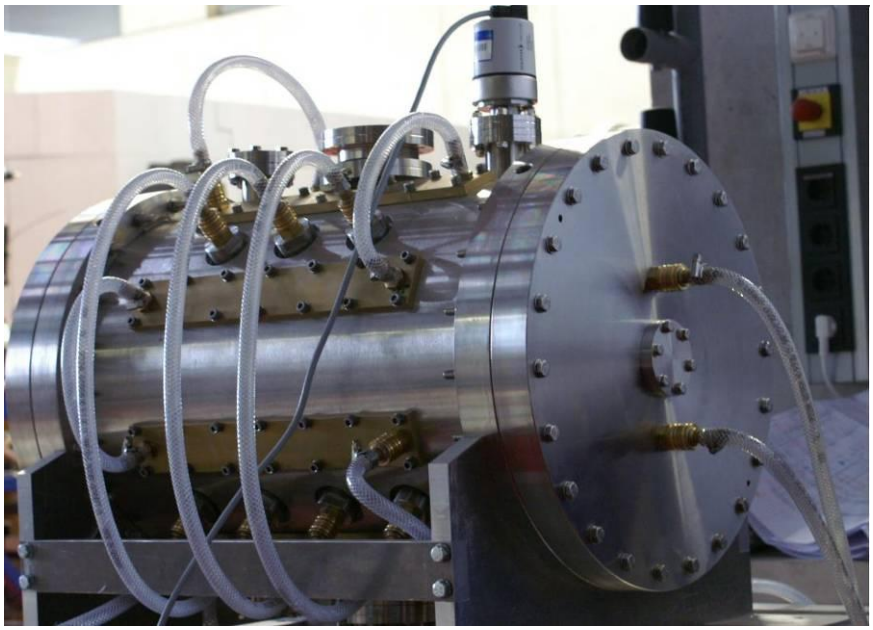

Fig.12: A view of a single CH-DTL where it is possible to see the cooling system.

3.2.3 The End Cells

Both IH and CH show naturally a cosine distribution of the electric field due their real resonant modes, respectively H_{111} and H_{211}: in order to approximate the 'zero mode' a tuning method has to be found.

In the IH, for instance, large undercuts are created in the girder at the cavity ends: the short circuit-action of the end walls with respect to H-modes is suppressed by that geometry if the undercuts are getting large enough.

In room temperature CH cavities, no girder can be located inside the cavity because this will lead to deformation of the outer cylinder during the welding procedure. Thus, the tuning should use a different strategy to decrease the resonant frequency at the cavity end.

The simplest way is to lengthen the last half drift tube increasing in this way the volume of the end cell; the radius of the last end half drift tubes can then be increasing so that not only the end cell are made resonant but, at the same time, they become large enough to host the magnetic element needed for beam focusing.

It is important to remark that since the electric field is strongly concentrated nearby the cavity axis, the increasing of radius of this large end half drift tubes will neither influence the shunt impedance nor the Q-value. In this way a very compact structure can be developed reducing the distance between adjacent tanks which helps the longitudinal beam dynamics since it profits a lot by a short distance between adjacent tanks.

3.3 RF Simulations

The RF properties of the cavity were simulated with the 3D code Microwave Studio: the attention was focused on the electric field distribution along the cavity, on the RF losses and on the strength of the coupling between the CH resonators.

As expected, in the frequency domain of interest there are two resonating modes close to each other: the operating mode, resonating at 325.2 MHz and the parasite one which occurs at 326.5

MHZ. The distance of 1.3 MHz from the operating mode ensures a safety margin in operation since the bandwidth of the klystron is 750 kHz.

The first mode, the 0 mode, is characterised by the oscillation in the E_{010} mode of the coupling cell: the current on the lens outer cylinder oscillates since the lens extremes at different potential and the magnetic field is responsible for the coupling with the CH resonators as explained in the previous section: in Fig.14 the magnetic flux is shown at half of the radius of the CH resonators.

The electric field distribution on the cavity axis is plotted on Fig.13 while Fig.14 shows the corresponding voltage distribution compared with the reference value as calculated by LORASR. As one can see from this picture the field distribution is rather balanced between each section and there is a satisfactory agreement between the voltage distributions. The Q-value results to be around 15300 which confirms the quality of the resonance scheme.

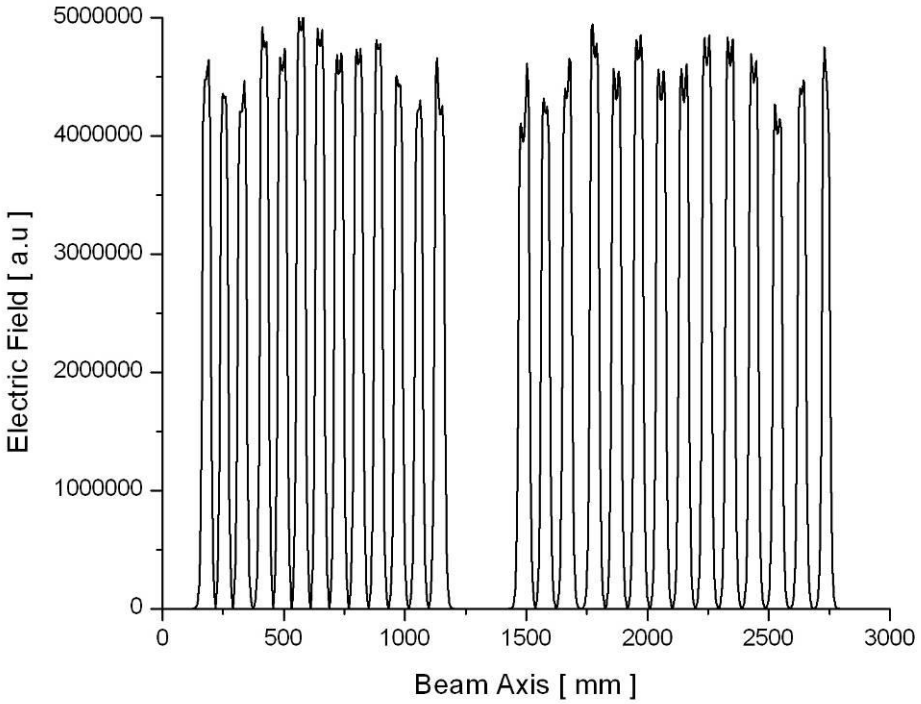

Fig.13:The electric field distribution as calculated by MWS.

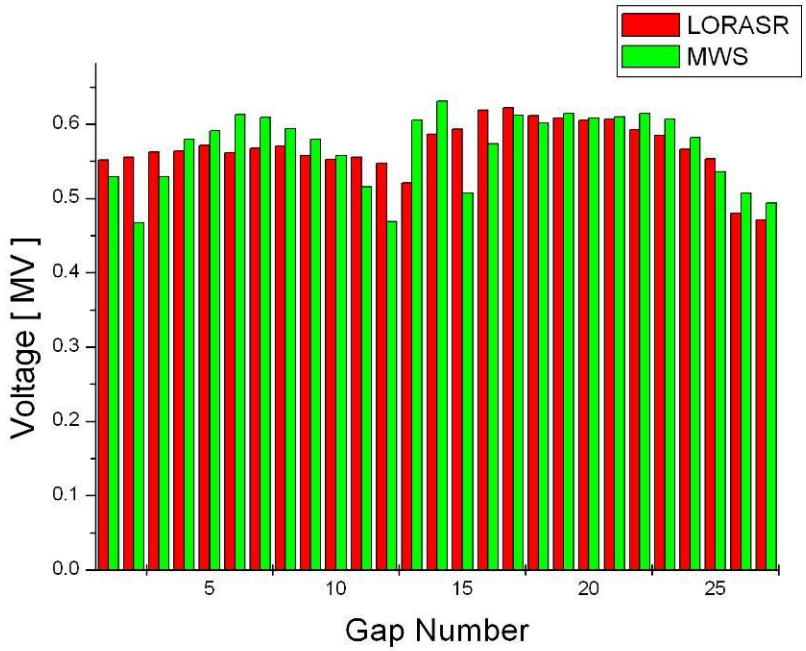

Fig.14: A comparison between the voltage distribution as calculated by Microwave Studio and by LORASR

The closest mode is the π/2 where the magnetic field line runs parallel and parallel along the single structure and the coupling between both resonators is extremely weak as one can see from Fig.15 where the field distribution on the cavity axis is shown.

This is a very important feature of the coupling scheme since it gives a natural hint where the structure must be coupled with the power supply. If the incoupling is in fact placed in the intertank section the parasite mode could be only weakly exited avoiding the risk of an overlapping between those two modes.

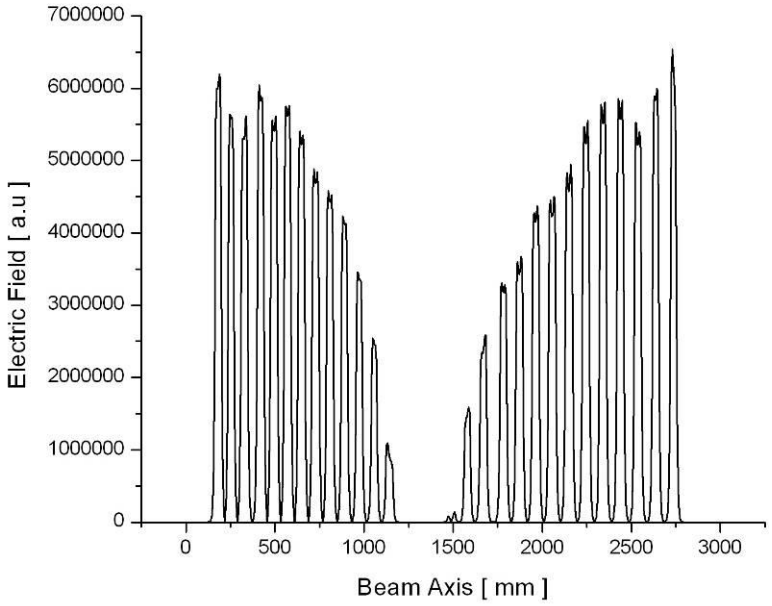

Fig.15: The electric field distribution of the first parasite mode

This concept becomes clear observing the magnetic field distribution in the middle plane of the cavity for the operating and for the parasite mode: as one can see from Fig.18 the magnetic field in the intertank section is three orders of magnitude lower than in the operational mode.

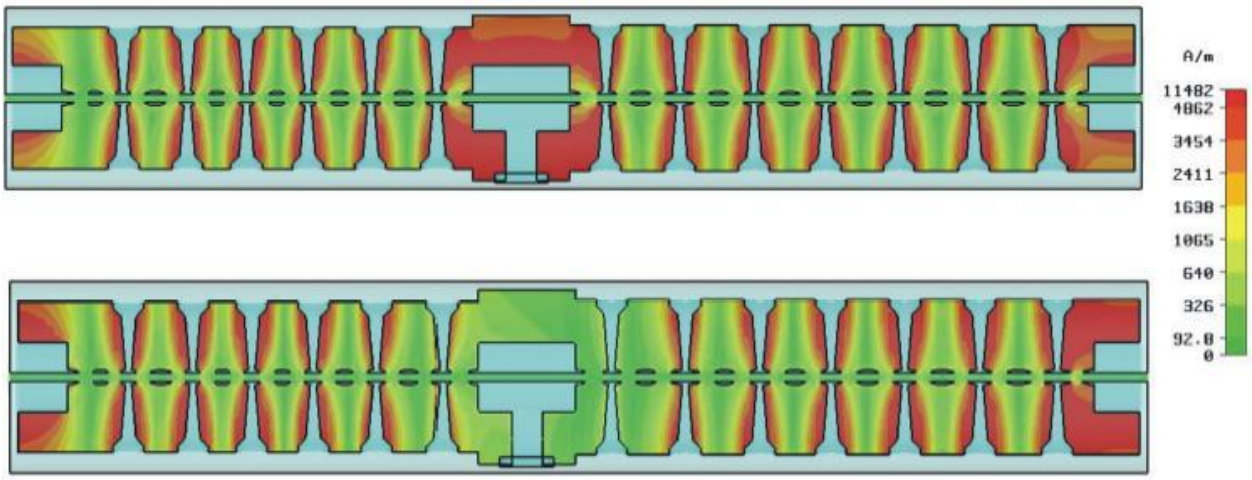

Fig.16: The magnetic field on the cavity middle plane for the 0 and for the π/2 mode.

4 Construction and test of the 1:2 scaled model

Even if the simulations performed with MWS result to be really promising, the complexity of such a resonator requires a deeper investigation that only an experimental campaign can ensure: for this reason a 1:2 scaled model has been built to test the main RF parameters such as resonance frequency, Q_0 value, shunt impedance and field distribution.

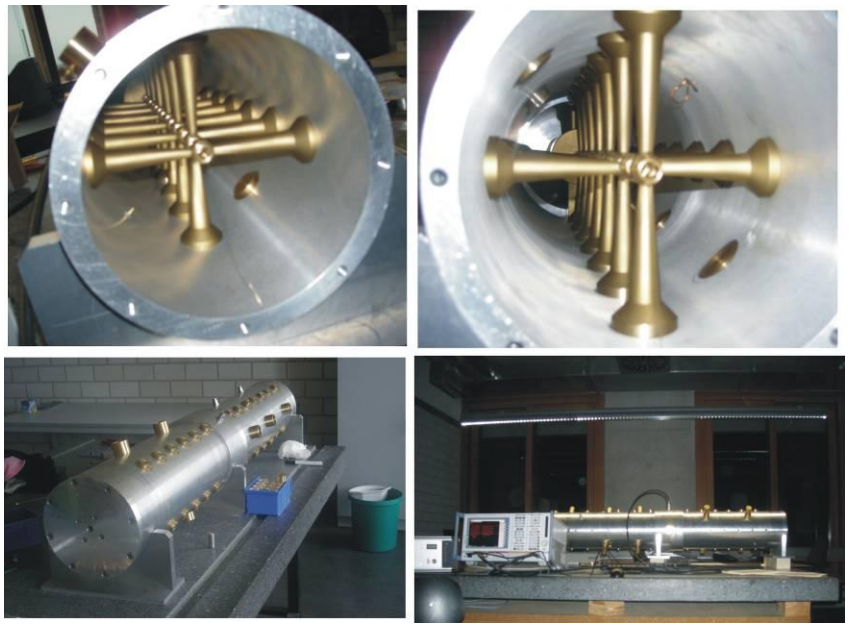

Fig.17:On top, two details of the cavity; bottom two photos of the closed cavity on the test bench

Fig.18: A detail of the incoupling cell including the dummy triplet

Fig.17 shows some details of the cavity: since the coupling between both resonators is rather sensitive to the radius of each single CH it was decided to equip the cavity with mobile plungers (15 mm in radius) which can be used to modify the field distributions and to drive the resonance frequency towards the desired value. The first section contains 2 couples of plungers which are mounted at 45° with respect to the stems axis while the second section has been equipped with other three couples.

One more plunger is located in the coupling cell at 90° with respect to the lens support.

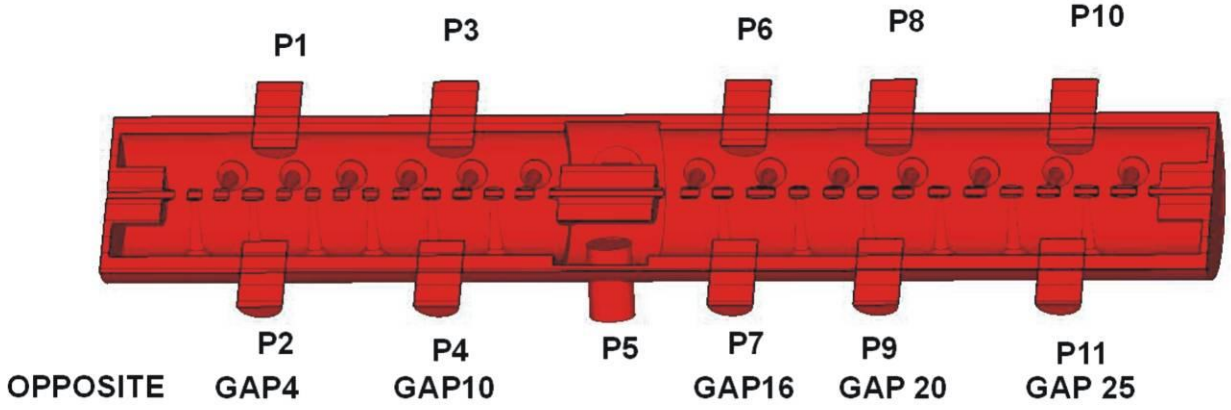

Fig.19: A longitudinal cut of the cavity showing the plunger positions

The outer cylinder is made in aluminium while the stems, the drift tubes and the dummy plungers are done in bulk messing. The drift tube can be screwed inside the stem and they can easily and rapidly exchange if needed.

The result of the first measurement is illustrated in Fig.20 and 21: the first cavity presents an overvoltage in the low energy end with a lack of voltage from gap 8 to 10; on the other side, the second resonator presents a lack of voltage at the high energy end.

The resonance frequency spectrum is in good agreement with the simulations: the 0 mode resonates at 652.64 MHz, the π/2 mode occurs at 653.98 MHz, while the H_{212} mode resonates at 658 MHz. The Q_0-value for the 0 mode results to be around 3500 and doesn't depend on the plungers position.

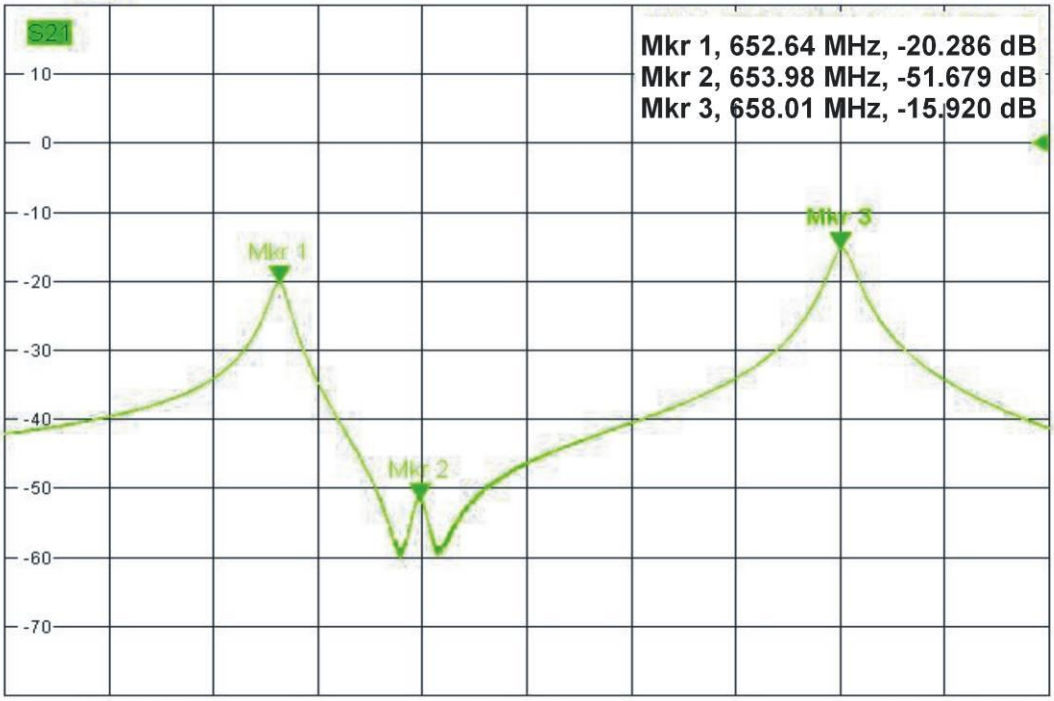

Fig.20: The frequency spectrum of the first distribution

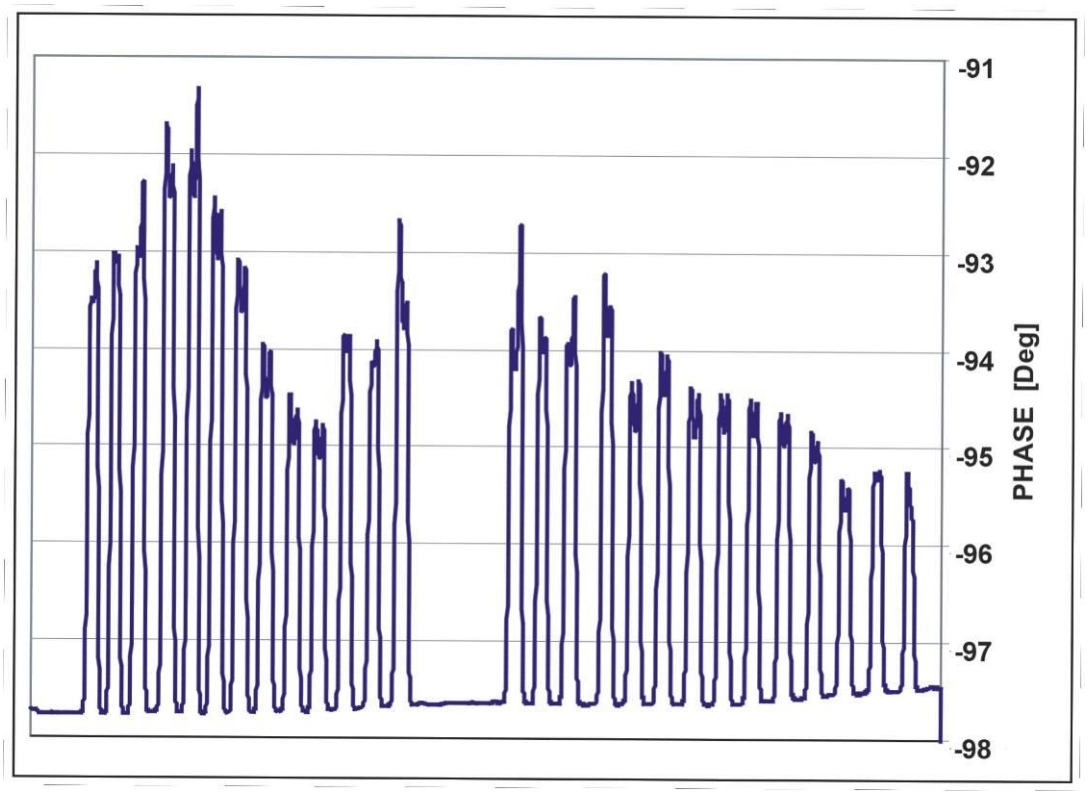

Fig.21: The phase distribution of the first measurements.

These results show a good agreement with the simulated value: the error in the resonance frequency of the 0 mode is 0.3 % while the π /2 is weakly exited as expected: to improve the field distribution, in a first step the gap length has been again modified and finally several plunger position were investigated to study the effect on the frequency spectrum and on the field distribution.

No. of tube	Length(designed) [mm]	Length (modified) [mm]
8	21.5	21.12
10	22.0	21.75
11	23.35	23.925

Tab.3: The changes in the drift tube length after the first measurement.

After the modification of the drift tubes in the first CH resonators, several configurations for the plunger positions were analyzed. Finally, the first couple of plunger were set 15 mm inside the cavity, the third plunger 8 mm leaving out its opposite, and, in the second resonator, only plungers number 6 and 7 were set 5 mm inside the cavity. With this configuration the effect of the plunger located in the coupling cell was investigated.

Tab.4 shows the effect of the plunger located in the coupling cell with respect to resonance frequency: as one can see it acts inductively increasing the resonance frequency of the 0 mode while it doesn't' effect the resonance frequency of the π /2 mode but it reduces more and more its amplitude.

When the plunger is completely inside the cavity the parasite mode vanishes: this is an extremely important effect which can be used to get rid of this mode during operation.

This result is of PARAMOUNTAL importance: the main problem of all coupled cavities is the distance between the desired operating mode and the parasites one: in our design this problem can be solved or at least, strongly reduce looking for a plunger configuration which results is a good field distribution and kills the closest parasite mode as well.

Plunger 5 [mm]	Freq. 0 Mode [MHz]	Freq. PI /2 Mode [MHz]
0	653.0	654.5
10	653.03	654.5
20	653.206	654.5
30	653.28	654.5
40	653.31	654.5
50	653.41	654.5
60	653.51	vanished

Tab4: The effect of the plunger located in the coupling cell.

Concerning the other plunger it was observed that the frequency of the operating mode tends to increase when they are pushed inside the cavity: this means that the plungers can only act inductively.

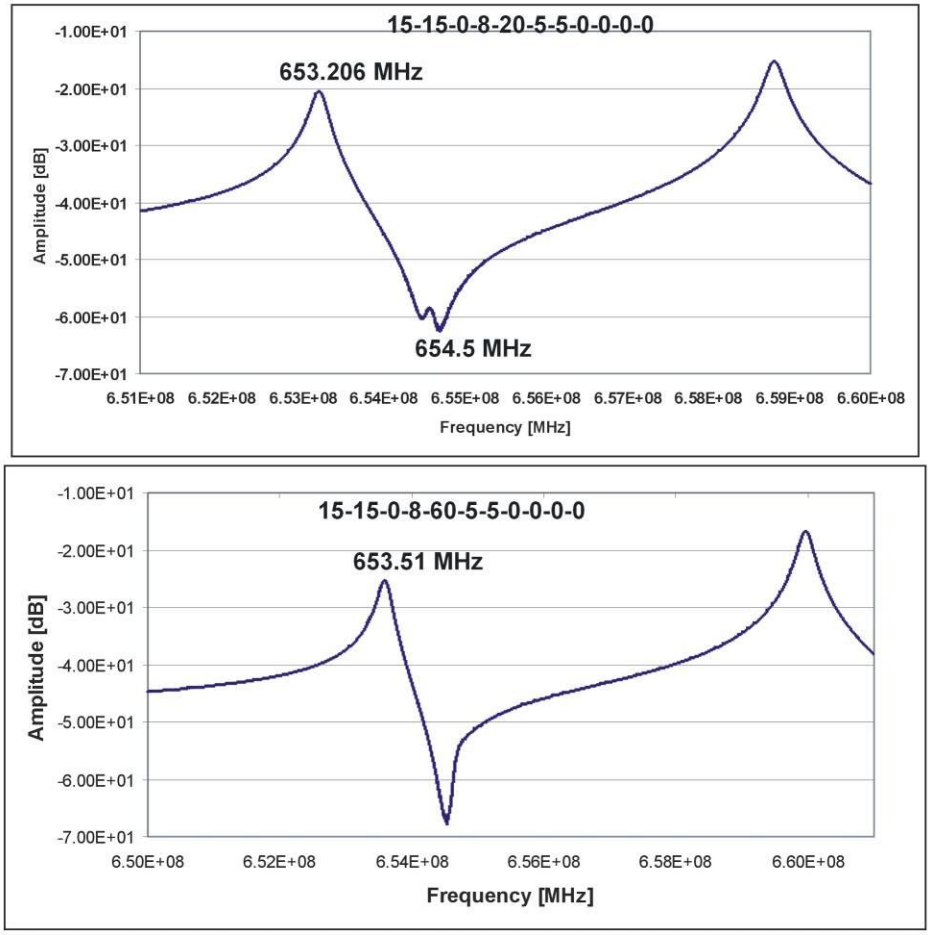

Fig.22: The effect of the plunger located in the coupling cell. The π /2 mode decrease increasing the depth of the plunger inside the cavity until it vanishes completely.

Concerning the field distribution the central plunger modifies the strength of the coupling gaps: this is well explained in the following examples which shows the field and voltage distributions for two positions of the central plungers, 20 and 40 mm respectively. As one can see both from the electric field and voltage distribution (Fig.23-24), the main effect of the central plunger is to reduce the voltage inside the coupling gaps. From this plots we can observe another interesting effect: the field distribution in both resonators presents a light undervoltage in the gaps close to the coupling cells which, instead, are strongly resonating. This can be explained considering the typical cosine profile of the field for an H-mode cavity which results in a lower voltage at the cavity end: in our structure, the 'zero mode' is then obtained on one side by use of the large half end drift tube and, on the other, by the coupling cell which oscillates in the classical E_{010} mode.

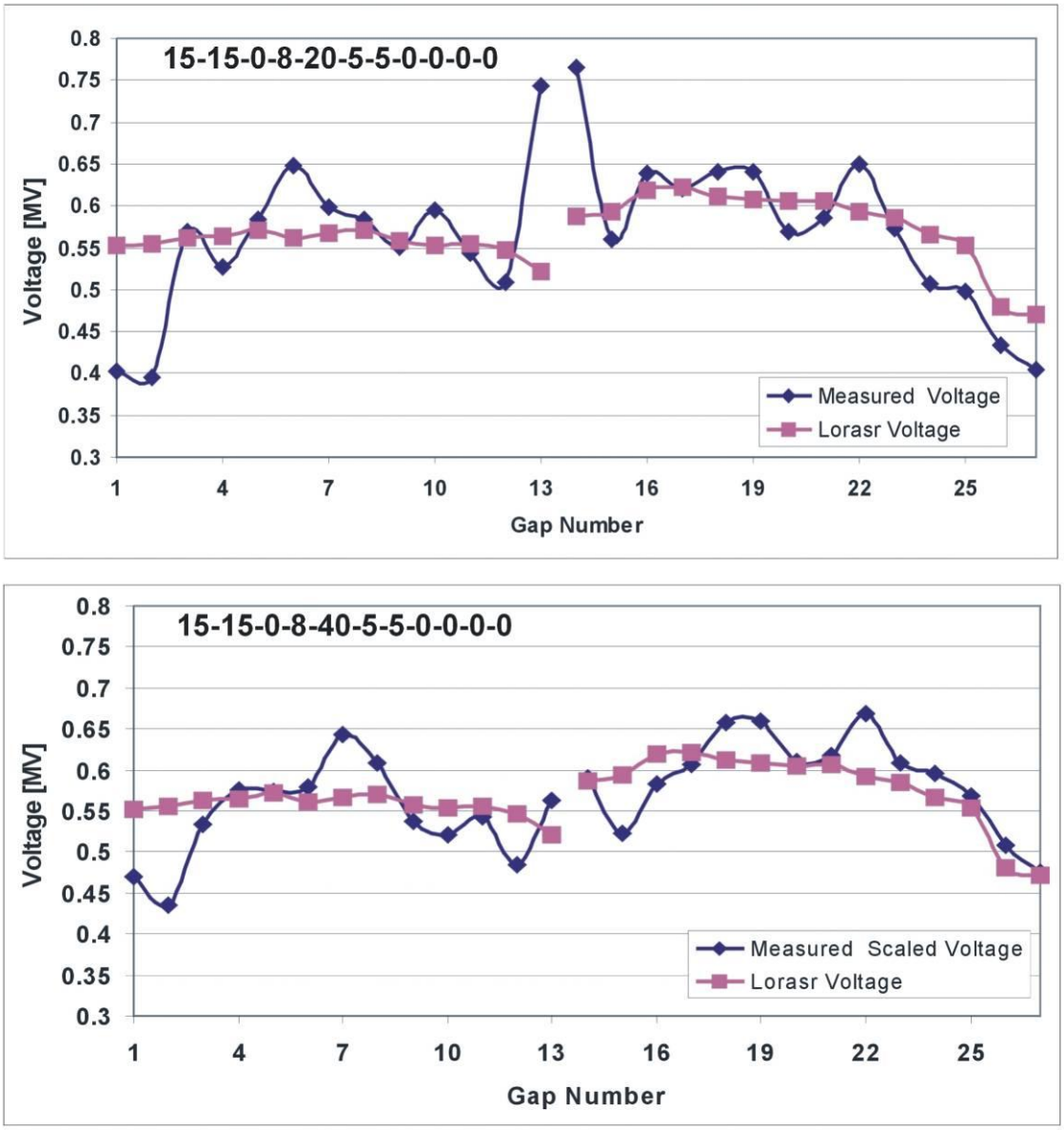

Fig.23: A comparison between the measured voltage distribution and the expectation values for two different positions of the plunger in the coupling cell, 20 and 40 mm, respectively.

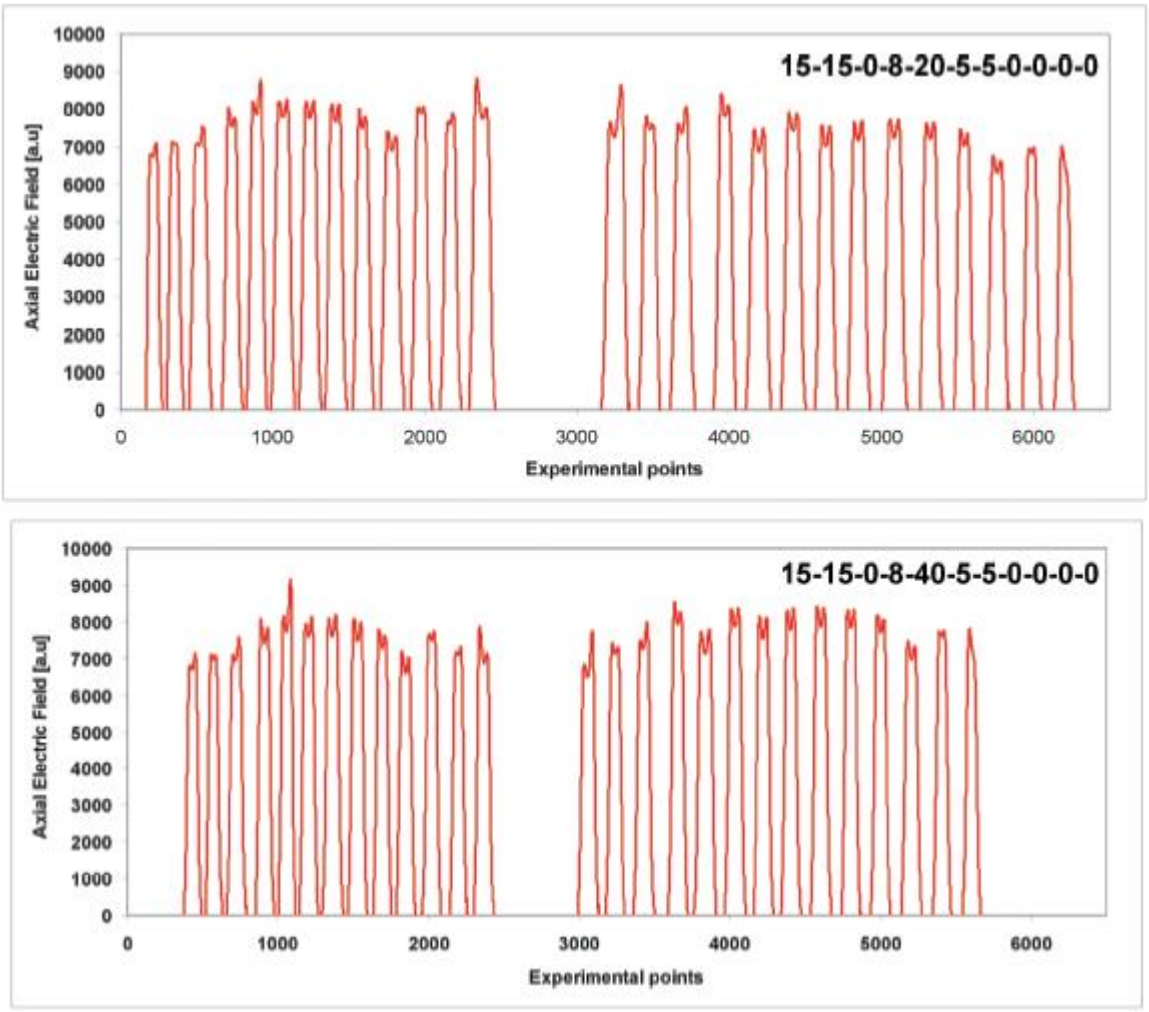

Fig.24: A comparison between the measured electric field distribution on the cavity axis for two different positions of the plunger in the coupling cell, 20 and 40 mm, respectively.

This latter case represents a really promising result and, for this reason, a detail summary is presented in Tab.5

Finally, from the bead pull measurement theory it is possible to evaluate the shunt impedance Z as

$$Z = \left(\int_0^l \sqrt{\frac{-\Delta\phi}{2\pi\omega r^3 \varepsilon_0}} \right)^2 \frac{1}{l}$$

which for this case results to be 107.85 MΩ/m$. Since the shunt impedance scales as the square root of the resonance frequency this value would correspond to 75.62 MΩ/m for a 325 MHz module, in good agreement with the simulated value 80.1 MΩ/m$.

Gap No.	LORASR VOLTAGE [MV]	Measured Voltage [MV]	Relative Error [%]
TANK 1			
1	552	470	-14.82
2	555	434	-21.71
3	563	533	-5.10
4	564	575	1.99
5	571	573	0.45
6	562	579	3.17
7	567	642	13.34
8	571	608	6.61
9	558	537	-3.71
10	553	521	-5.70
11	555	542	-2.25
12	547	484	-11.43
13	521	562	8.02
TANK 4			
14	587	589	0.44
15	594	521	-12.08
16	619	583	-5.66
17	622	606	2.52
18	614	657	7.44
19	608	660	8.53
20	605	610	0.80
21	607	618	1.91
22	592	669	12.94
23	585	608	4.09
24	565	595	5.16
25	555	568	2.78
26	480	508	5.93
27	471	474	0.79

Tab.5: The experimental result for the voltage distribution with the central plunger 40 mm down in the cavity

Acknowledgements

We acknowledge the support of the European Community-Research Infrastructure Activity under the FP6 “Structuring the European Research Area” programme (CARE, contract number RII3-CT-2003-506395)